Expected radiation damage of reverse-type APDs for the Astro-H mission

2012 JINST 7 P06001

(http://iopscience.iop.org/1748-0221/7/06/P06001)

PUBLISHED BY IOP PUBLISHING FOR SISSA MEDIALAB

RECEIVED: *April 16, 2012*
ACCEPTED: *May 7, 2012*
PUBLISHED: *June 1, 2012*

Expected radiation damage of reverse-type APDs for the Astro-H mission

J. Kataoka,[a,1] T. Saito,[a] M. Yoshino,[a] H. Mizoma,[a] T. Nakamori,[a] Y. Yatsu,[b] Y. Ishikawa,[c] Y. Matsunaga,[c] H. Tajima,[d] M. Kokubun[e] and P.G. Edwards[f]

[a] *Research Institute for Science and Engineering, Waseda University, 3-4-1, Okubo, Shinjuku, Tokyo 169-8555, Japan*
[b] *Tokyo Institute of Technology, 2-12-1 Ookayama, Meguro, Tokyo,152-8551, Japan*
[c] *Solid State Division, Hamamatsu Photonics K.K., Hamamatsu, Shizuoka, Japan*
[d] *Solar Terrestrial Environment Laboratory, Nagoya University, Nagoya, Aichi, 464-8601, Japan*
[e] *Institute for Space and Astroautical Science/JAXA, 3-1-1 Fuchinobe, Sagamihara, Kanagawa, 229-8510, Japan*
[f] *Australia Telescope National Facility, CSIRO Astronomy and Space Science, Epping NSW 1710, Australia*

E-mail: kataoka.jun@waseda.jp

ABSTRACT: Scheduled for launch in 2014, Astro-H is the sixth Japanese X-ray astronomy satellite mission. More than 60 silicon avalanche photodiodes (Si-APDs; hereafter APDs) will be used to read out BGO scintillators, which are implemented to generate a veto signal to reduce background contamination for the hard X-ray imager (HXI) and a soft gamma-ray detector (SGD). To date, however, APDs have rarely been used in space experiments. Moreover, strict environmental tests are necessary to guarantee APD performance for missions expected to extend beyond five years. The radiation hardness of APDs, as for most semiconductors, is particularly crucial, since radiation in the space environment is severe. In this paper, we present the results of radiation tests conducted on reverse-type APDs (provided by Hamamatsu Photonics) irradiated by gamma rays (^{60}Co) and 150 MeV protons. We show that, even under the same 100 Gy dose, high energy protons can cause displacement (bulk) damage in the depletion region and possibly change the activation energy, whereas gamma-ray irradiation is less prone to cause damage, because ionization damage dominates only the surface region. We also present quantitative guidance on how to estimate APD noise deterioration over a range of temperatures and radiation doses. As a practical example, we discuss the expected degradation of the BGO energy threshold for the generation of veto signals, following several years of Astro-H operation in Low Earth Orbit (LEO), and directly compare it to experimental results obtained using a small BGO crystal.

KEYWORDS: Space instrumentation; Gamma detectors; Photon detectors for UV, visible and IR photons (solid-state) (PIN diodes, APDs, Si-PMTs, G-APDs, CCDs, EBCCDs, EMCCDs etc); X-ray detectors and telescopes

[1] Corresponding author.

doi:10.1088/1748-0221/7/06/P06001

Contents

2012 JINST 7 P06001

1 Introduction

The avalanche photodiode (APD; [1]) is a compact, high-performance light sensor, which is increasingly being applied in various fields of experimental physics (e.g., [2]). Reverse-type (or buried junction) APDs are particularly advantageous in detecting weak scintillation light signals with excellent noise performance, thanks to their narrow high-field multiplying region close to the front end [3–5]. In ground experiments, more than 140,000 reverse-type APDs (5x5 mm in size) were fully implemented to read out $PbWO_4$ scintillators on the calorimeter for the Compact Muon Solenoid (CMS) experiment at CERN's Large Hadron Collider (LHC) [6–9]. Despite the very harsh APD operating conditions, namely a very high magnetic field environment and high levels of radiation, the reverse-type APDs produced by Hamamatsu worked well, and earned a prestigious CERN Crystal Award in 2003. These APDs are also attractive in other fields, especially nuclear medicine. The advantages of pixel miniaturization pave the way for APD applications in dense position-sensitive detectors, and so APD-based PET scanners for future applications in nuclear medicine are feasible [10–18].

APDs also have a range of applications in LIght Detection And Ranging (LIDAR), and optical communications [19, 20]. Likewise, there are plans to use APDs on astrophysical satellites such as Astro-H [21] and ATHENA/IXO [22], since APDs are much more compact than traditional photomultipliers (PMTs), and operate at a relatively low bias voltage and with low power consumption. Although the gain characteristics of APDs are quite temperature-dependent, various temperature-compensation systems have been proposed and successfully demonstrated (e.g., [23]). To validate the initial use of APDs to detect radiation in a space experiment, we developed the pico-satellite Cute-1.7+APD II ($10\times15\times20$ cm^3 in size; 5 kg in mass) that was successfully launched in April

2008 [24]. Three years on, the mission continues to provide data on the distribution of low energy particles (both electrons and protons) trapped in Low Earth Orbit (LEO), including the South Atlantic Anomaly (SAA) as well as auroral bands, with a minimum detectable energy of 9.2 keV [25].

Two instruments on-board the Astro-H satellite — the hard X-ray imager (HXI; [26]) and soft gamma-ray detector (SGD; [27]) — will carry more than 60 APDs for highly sensitive observations in LEO. The reverse-type APDs will be used to read out scintillation light from the BGO "active shield" around the main detectors, which comprise Si-Pad, DSSD (Double Sided Silicon Detector), and CdTe detectors. The active shield generates veto signals for efficient background rejection. To maximize background rejection, it is crucial to minimize the energy threshold of the BGO shield with a dedicated analog circuit [4, 28]. However, APD damage caused by radiation, in terms of increased dark (or leakage) current and degraded quantum efficiency (QE), may significantly impair the overall noise performance of the detector.

This study was performed to quantitatively evaluate the APD sensor damage when exposed to radiation up to 100 Gy, over the temperature range -20°C to $+20^{\circ}$C. The results are applicable to the Astro-H mission, although some instruments and thermal designs are still being investigated or optimized. Here, we present the results of various tests conducted on APD flight sensors for Astro-H that were irradiated with gamma rays (^{60}Co) and high energy protons (150 MeV) for total doses of 100 Gy. We believe this approach is simple, straightforward, and easily applicable to APDs used in particle accelerator facilities and other space missions in the near future.

2 Radiation test of APD

2.1 Reverse-type APD for Astro-H

The reverse-type APDs described in this paper, S11673-01(X), were developed based on the S8664 series (Hamamatsu) technology, but specifically customized for use in the Astro-H HXI/SGD. In particular, we adopted a silicone elastomer encapsulant in place of the standard, hard optical epoxy window. The optical entrance window material had to be changed after the hard epoxy optical window suffered cracking and delamination from BGO scintillator surfaces during qualification thermal cycling (between $+45^{\circ}$C and -35°C; 20°C/hr, 1hr dwell, 20 cycles), resulting in a substantial degradation of the light output signals from the APDs [28]. We also made a minor change to the ceramic case to reduce internal background interference, by adopting a Potassium-free package. Moreover, the anode and cathode were double-wired for redundancy and the anode and cathode grid optimally positioned to prevent electrical discharge in space.

This APD sensor is incorporated into a thin aluminum electromagnetic (EM) shield 200 μm thick. Figure 1(a) shows a picture of the APD (with and without the EM shield) and one of the BGO crystals used to form an active shield for the Astro-H SGD. The current thermal design of the Astro-H HXI/SGD predicts APD operation at around -15°C. Table 1 lists the design parameters, dark noise and gain characteristic of the two APD devices used in the beam tests described in this paper (either ^{60}Co or proton). Figure 1(b) gives a schematic view of the internal structure of the Hamamatsu reverse-type APDs. The basic performance and characteristics of reverse-type APDs (Hamamatsu S8664 series) are also documented in detail elsewhere [3–5].

2012 JINST 7 P06001

Table 1. Parameters of the Hamamatsu reverse-type APD for Astro-H.

	FM9	FM10
Surface Area	10×10 mm^2	10×10 mm^2
Window	Si-resin	Si-resin
Dark current (M=50, 25°C) I_d	14 nA	17 nA
Break-down voltage: V_{brk} (25°C)	451 V	452 V
Operation bias: $V_{M=50}$	406 V	406 V
Capacitance: C_{det}	270 pF	270 pF

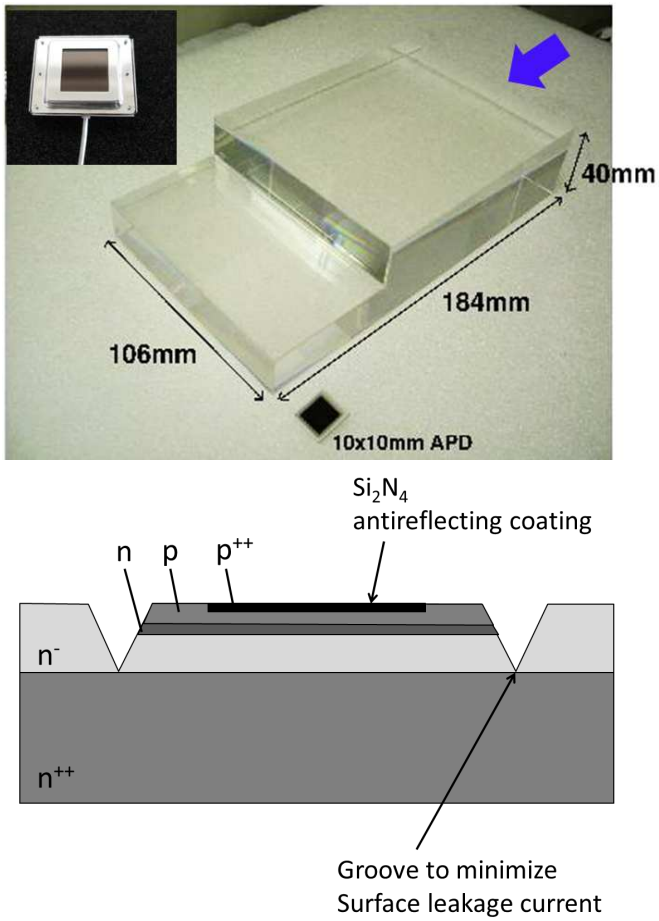

Figure 1. *Top*: (a) A picture of the reverse-type APD (10×10 mm^2) developed for the Astro-H mission, and a sample BGO scintillator for the active shield of the SGD. The BGO surface to which APD is glued is indicated by the blue arrow. *Bottom*: (b) Internal structure of reverse-type APDs produced by Hamamatsu (S8664 series).

2012 JINST 7 P06001

2.2 ^{60}Co irradiation

It is generally thought that ^{60}Co gamma radiation causes ionization damage in the surface region of the device. Displacement damage caused by gamma rays, however, occurs indirectly due to Compton electrons (with a 1.2 MeV maximum energy), but only on a very small scale compared to protons (e.g., [29–31]). Si recoil energies can generate a maximum of one or two displaced atoms per scattered electron [32].

All irradiation was performed at the Tokyo Institute of Technology in Tokyo, Japan. For this experiment, we used the FM10 APD sensor listed in table 1. The total dose was 100 Gy with a dose rate of ∼0.05 Gy/s. The dose uncertainty for the irradiation was estimated to be less than 5%. The APDs were irradiated in the dark with no electrical connections, but similar results were obtained when operating equivalent APDs at a nominal high gain value at 400 V. It should also be noted that following irradiation, dark current declines over time, due to the well-known annealing effect. However, this decrease occurs over several weeks, a period much longer than that of the irradiation. The time elapsed between ^{60}Co gamma-ray irradiation and post-irradiation measurements was about 24 hr.

As we can see in figure 2(a)−(c), 100-Gy gamma irradiation leaves most APD parameters (e.g., break-down voltage, gain characteristics, QE) unchanged except for the dark current. Here, the gain and dark current were measured at temperatures of −20, −15, −10 and +20 °C, but QE was only measured at +25°C. Note that the slope of the $M - I_d$ curve (figure 2(b)) is *flatter* after the gamma-ray irradiation. Qualitatively, this is well understood if the unmultiplied component of the dark current, i.e., the surface current of the APD device, increases after gamma-ray irradiation. Moreover, the ratio of dark current before and after irradiation is only marginally temperature-dependent (4.4 at +20°C, and 5.6 at −20°C). As we see below, this suggests that the activation energy in the device does *not* change substantially due to ionization damage caused by ^{60}Co gamma-ray irradiation.

2.3 Proton irradiation

In contrast to gamma-ray irradiation, displacement (bulk) damage is the major radiation effect observed with protons rather than ionization (surface effect), which may affect bulk device parameters [29, 30, 33]. To evaluate the degradation of reverse-type APDs caused by proton irradiation, we irradiated APDs with 150 MeV protons at the HIMAC (Heavy Ion Medical AcCelerator) high-energy ion beam facility in Chiba, Japan, as a part of a collaborative research experiment (research number P258). For this experiment we used the FM9 APD sensor, the properties of which are listed in table 1. The total dose was 100 Gy with a dose rate of ∼0.1 Gy/s. The dose uncertainty for the irradiation was estimated to be less than 10%. The APDs were irradiated in the dark with no electrical connections. Again, the gain and dark current were measured at temperatures of −20, −15, −10 and +20 °C, but QE was only measured at +25°C.

As is apparent from figure 3(a), 100-Gy proton irradiation does not change the gain characteristics of the APD, as was the case for gamma irradiation. However, QE degrades substantially above 600 nm (figure 3(c)), suggesting damage generated relatively deep in the bulk of the detector, rather than on the device surface. This is consistent with the slope of the $M - I_d$ curve (figure 3(b)) becoming *steeper* after proton irradiation, suggesting a substantial increase in bulk current, which

2012 JINST 7 P06001

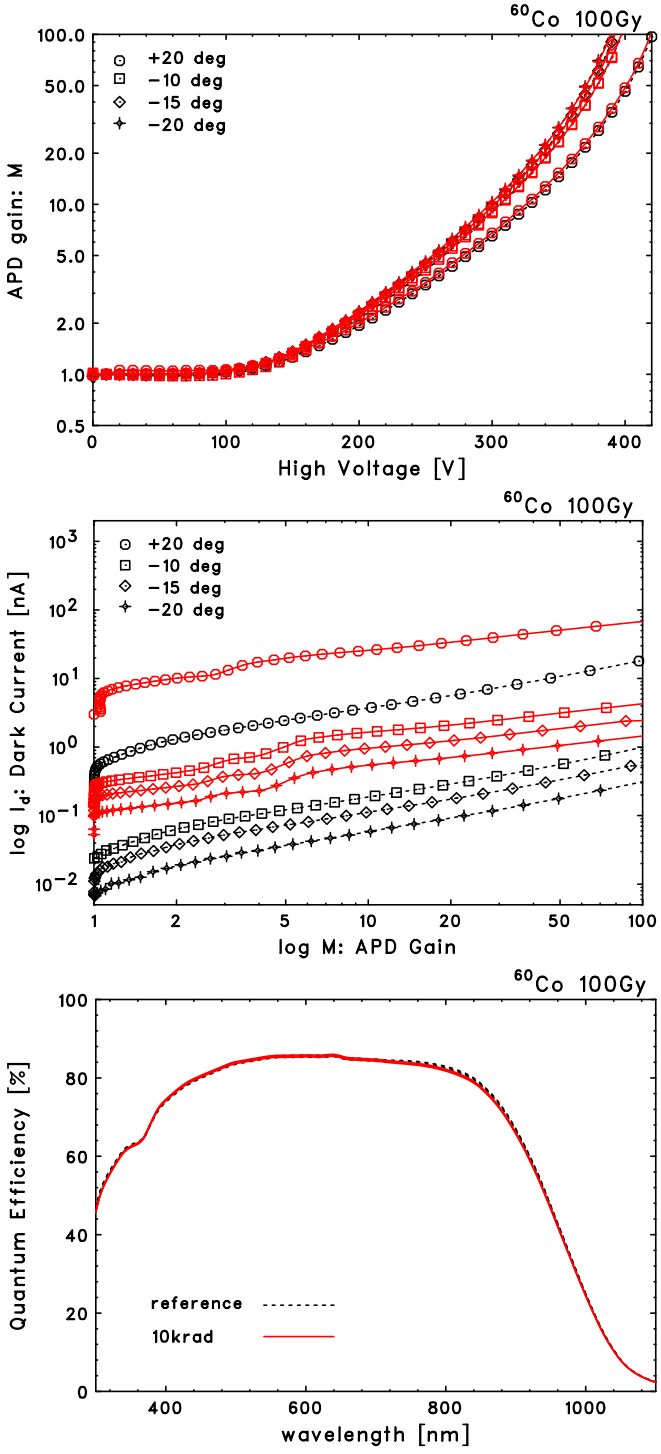

Figure 2. Characteristics of the reverse-type APD (FM10) before and after gamma-ray irradiation. *Top*: (a) gain vs. bias voltage, *middle*: (b) dark current vs. gain, and *bottom*: (c) QE vs. wavelength. *Black* (dashed lines) denote data before irradiation. *Red* (solid lines) denote data after 100-Gy irradiation.

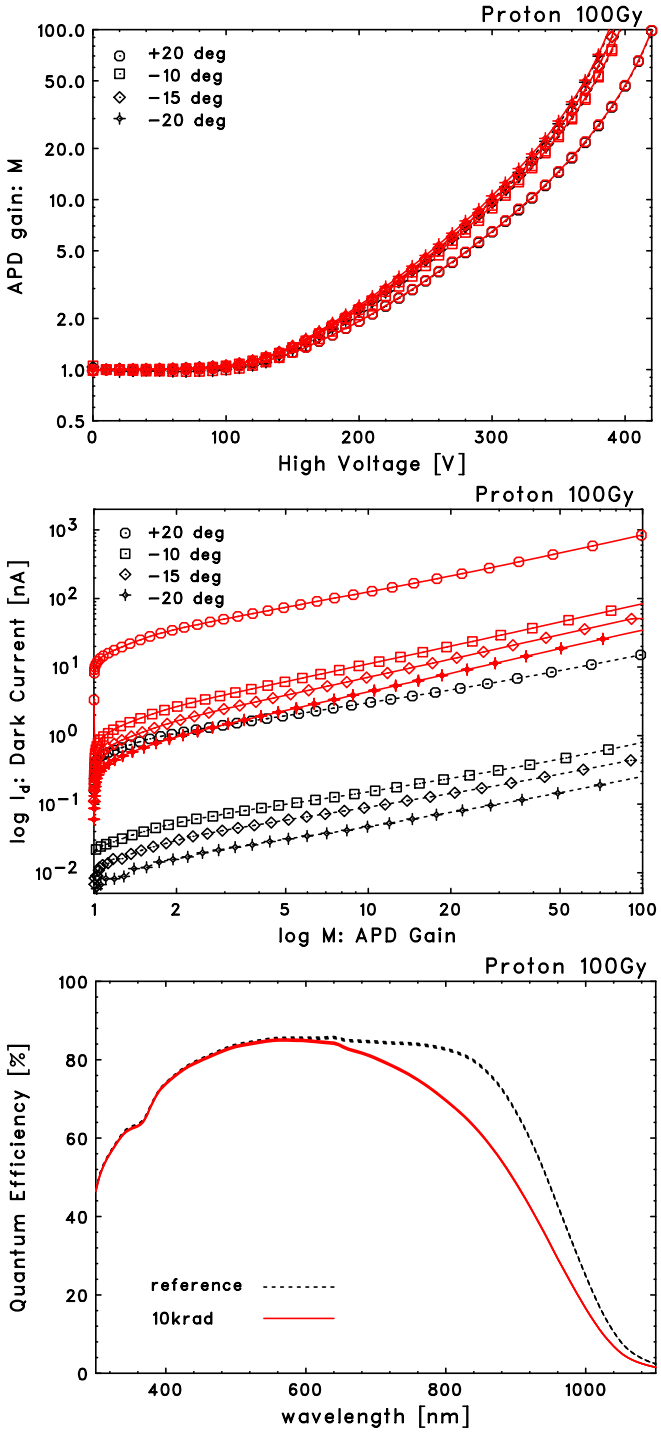

Figure 3. Characteristics of the reverse-type APD (FM9) before and after 150 MeV proton irradiation. *Top*: (a) gain vs. bias voltage, *middle*: (b) dark current vs. gain, and *bottom*: (c) QE vs. wavelength. *Black* (dashed lines) denote data before irradiation. *Red* (solid lines) denote data after 100-Gy irradiation.

2012 JINST 7 P06001

is the multiplied component of the APD dark current. Moreover, the ratio of dark current before and after irradiation is quite temperature-dependent (54 at $+20^{\circ}$C and 125 at -20°C). This suggests a significant change in activation energy due to displacement damage caused by proton irradiation.

3 Discussion

3.1 Estimation of activation energy in the APD

To quantitatively evaluate the radiation effects caused by either gamma rays or protons, we initially distinguish "surface" and "bulk" components in a measured APD dark current before irradiation (0 Gy). The APD dark current is generated both from leakage at the diode surface and from electron-holes thermally generated within the bulk of the silicon, which are then multiplied in the gain region. Consequently the total dark current of the APD measured at a certain temperature T (in K), is given by

$$I_d(T,M) = I_{ds}(T) + M \times I_{db}(T) \tag{3.1}$$

where I_{ds} and I_{db} denote the surface and bulk currents, respectively, and M denotes the APD gain. The temperature dependence of the APD dark current is generally given by

$$I_{ds}(T) \propto T^2 \exp(-\varepsilon_s/kT) \tag{3.2}$$

$$I_{db}(T) \propto T^2 \exp(-\varepsilon_b/kT) \tag{3.3}$$

where k denotes the Boltzmann constant, and ε_s and ε_b are the activation energies corresponding to the surface and bulk components of the dark current [34–36]. Obviously, these values may vary with the device structure and possibly with the impurity concentration in the APD. For example, $\varepsilon_s \simeq 0.70$ eV and $\varepsilon_b \simeq 0.55$ eV are reported for Si-APDs manufactured by Perkin Elmer [37].

To calculate I_{db} and I_{ds}, we can take certain gains M_A and M_B (where $M_B > M_A$) from the M-I_d curve (figures 2(b) and 3(b)) measured at a certain T. Note that M_A and M_B should be sufficiently large that the APD device is fully depleted and eq. (3.1) is a good expression of measured data ($\gtrsim$ 20 for the case of reverse type APDs used in this paper). Hence we can estimate I_{ds} and I_{db} as

$$I_{db}(T) = \frac{I_d(T,M_B) - I_d(T,M_A)}{M_B - M_A} \tag{3.4}$$

$$I_{ds}(T) = I_d(T,M_A) - M_A \times I_{db}(T) \tag{3.5}$$

Next, by measuring I_{db} and I_{ds} at different absolute temperatures T_1 and T_2 (where $T_2 > T_1$), we can evaluate the activation energy as

$$\varepsilon_s = \frac{kT_1T_2}{T_2 - T_1} \log\left[\left(\frac{T_1}{T_2}\right)^2 \frac{I_{ds}(T_2)}{I_{ds}(T_1)}\right] \tag{3.6}$$

$$\varepsilon_b = \frac{kT_1T_2}{T_2 - T_1} \log\left[\left(\frac{T_1}{T_2}\right)^2 \frac{I_{db}(T_2)}{I_{db}(T_1)}\right] \tag{3.7}$$

For example, considering the APD FM10 sensor before irradiation. From figure 2, and eqs. (3.4) and (3.5), we obtain $I_{ds} = (3.83\pm0.32)\times10^{-2}$ nA, $I_{db} = (2.80\pm0.05)\times10^{-3}$ nA at $T_1 = 253$ K (-20°C), and $I_{ds} = 2.54\pm0.18$ nA, $I_{db} = (1.61\pm0.03)\times10^{-1}$ nA at $T_2 = 293$ K (+20°C),

2012 JINST 7 P06001

respectively, where the uncertainties here were estimated by taking various different M_A and M_B that satisfy $20 \lesssim M_A < M_B \lesssim 100$, for the calculation. By comparing I_{ds} and I_{ds} at T_1 and T_2, ε_s and ε_b can easily be derived as $\varepsilon_s = 0.62 \pm 0.03$ eV and $\varepsilon_b = 0.60 \pm 0.03$ eV (see, eqs. (3.6) and (3.7)). Also note that the activation energies derived here are unaffected, within errors, by the exponent 2 in eqs. (3.2) and (3.3). This is because the rapid change of dark current with temperature is mainly due to the exponential term $\propto \exp(-\varepsilon/kT)$, rather than the more slowly varying $\propto T^2$ term.

3.2 Effects of radiation damage

The above calculations also apply to APDs after irradiation. For the gamma-ray irradiated FM10 APD, we measured the dark current as shown in figure 2 at various temperatures from -20 to $+20^\circ$C. By comparing I_{ds} and I_{db} measured at $T_1 = 253$ K and $T_2 = 293$ K, we obtain $\varepsilon_s = 0.58 \pm 0.03$ eV and $\varepsilon_b = 0.56 \pm 0.03$ eV after the 100-Gy gamma-ray irradiation. These results are slightly smaller, but marginally consistent with the pre-irradiation values. We also note that I_{ds} increased by factors of 10.4 and 14.0, measured at $+20^\circ$C and -20°C, respectively, whereas I_{db} increased by factors of 2.54 and 3.27 at the same temperatures. The results correlate well with our expectation that gamma-ray radiation mainly damages the surface region of the device via ionization.

Similarly, we can evaluate the damage caused by proton irradiation by referring to FM9 data. By comparing I_{ds} and I_{db} measured at $T_1 = 253$ K and $T_2 = 293$ K, we obtain $\varepsilon_s = 0.46 \pm 0.03$ eV and $\varepsilon_b = 0.48 \pm 0.03$ eV, respectively, after irradiation. The results confirm a significant change of activation energy, as briefly commented in section 2.3. Moreover, I_{ds} increased by factors of 18.6 and 48.8 as measured at $+20^\circ$C and -20°C, respectively, whereas I_{db} increased by factors of 65.7 and 149 at the same temperature. Again, this is consistent with the general expectation of protons causing greater damage and resulting in an increase in the bulk current, rather than the surface current.

3.3 Expected degradation of the BGO threshold for Astro-H

In the Astro-H mission, the total radiation dose is expected to be 50 to 100 Gy (depending on the shielding structure and actual electron/proton flux) over the nominal five-year mission, based on the latest LEO plan of an altitude of $\sim$550 km and an inclination of 31°. We predict about 5% of the total dose will be attributable to high energy protons; namely a total of 3 to 5 Gy. Using the experimental data given in the previous sections, we attempted to predict the degradation of the BGO energy threshold (i.e., convolution of total noise increase due to APD degradation and electronic noise) at arbitrary temperature T and radiation dose D. The following equations estimate the electronic noise of the APD system (in units of electrons, FWHM; e.g., [38]).

$$\Delta^2_{\rm noise} = 2.35^2 \left[\frac{2}{e} \left(\frac{I_{ds}}{M^2} + I_{db} F \right) \tau + 4kTR_s \frac{C^2_{det}}{M^2} \frac{1}{\tau} \right] \tag{3.8}$$

$$\simeq \left[\Delta^2_{\rm dark}\right] + \left[\Delta^2_{CSA}\right] \tag{3.9}$$

where e denotes the electron charge, F the excess noise factor (we assume $F = 2.0$ for the S8664 series APD, as reported in the literature [4]), C_{det} the detector capacitance including the signal cable, R_s the preamplifier series noise resistance, and τ (here, we assume $\tau = 1\mu$s; [28]) the shaping time constant.

2012 JINST 7 P06001

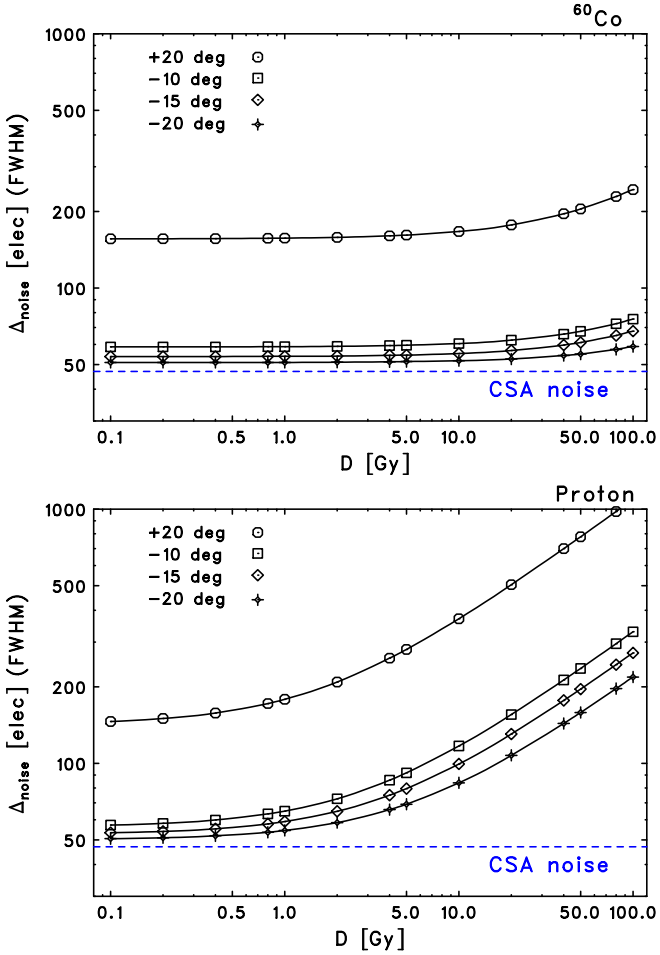

Figure 4. Expected electronic noise degradation as a function of radiation dose D at various operational temperatures (-20, -15, -10 and $+20^{\circ}$C) assuming the APD read out system for the Astro-H mission. (*top*): (a) Gamma rays, (*bottom*): (b) Protons. The errors of each data point are smaller than the symbol size.

The first term of eq. (3.8) represents noise originating from the APD dark current (shot noise; $\Delta^2_{\rm dark}$), whereas the second term represents noise due to the preamplifier (parallel and serial noise; Δ^2_{CSA}), which simply depends on the preamplifier's characteristics and parallel capacitance. From the parallel and serial noise measured directly on the Astro-H HXI/SGD, we obtain Δ_{CSA} = 47 electrons for a shaping time of 1 μs [28]. For APD noise, we obtain $\Delta_{\rm dark}$ = 138 electrons and 19.7 electrons as measured at $+20^{\circ}$C and -20°C, respectively, for the FM10 before gamma-ray irradiation. Therefore, we expect most electronic noise to be attributable to APD dark current at $+20^{\circ}$C ($\Delta_{\rm dark} \simeq 3.0\times\Delta_{CSA}$), but parallel and serial noise to dominate at -20°C ($\Delta_{CSA} \simeq 2.4\times\Delta_{\rm dark}$) before irradiation.

We can apparently extend this approach to an arbitrary radiation dose D and temperature T simply by replacing I_{ds} and I_{db} in eq. (3.8). For simplicity, we assumed the dark current increased linearly with the radiation dose. This was supported by our own follow-up experiments, as well as reports in the literature (e.g., [33]; see section 3.4 for further comments on annealing effects).

2012 JINST 7 P06001

The current thermal design of the Astro-H HXI/SGD predicts APD operation at around -15°C; therefore, we hereafter assumed T = 258 K. From the irradiation results of the FM10, we can infer that APD dark current at arbitrary dose D Gy (due to gamma rays) is expressed as

$$I_{ds}(D) = I_{ds,0} + D \times \Delta I_{ds} \tag{3.10}$$

where ΔI_{ds} = (8.60$\pm$0.43)$\times 10^{-3}$ nA/Gy and $I_{ds,0}$ (= (7.90$\pm$0.60)$\times 10^{-2}$ nA) denotes the surface current before irradiation. For the bulk current, we obtain

$$I_{db}(D) = I_{db,0} + D \times \Delta I_{db} \tag{3.11}$$

where ΔI_{db} = (1.20$\pm$0.06)$\times 10^{-4}$ nA/Gy and $I_{db,0}$ (= (4.90$\pm$0.09)$\times 10^{-3}$ nA) denotes the bulk current before irradiation.

Similarly for proton irradiation, we obtain ΔI_{ds} = (2.90$\pm$0.15)$\times 10^{-2}$ nA/Gy and ΔI_{db} = (5.20$\pm$0.26)$\times 10^{-3}$ nA/Gy respectively. Using these dark currents as input parameters in eq. (3.8), we can easily estimate the total electronic noise for arbitrary dose D. figures 4(a) and (b) give separate results for gamma rays and protons, as functions of D at various operating temperatures. The degradation caused by protons will clearly have a far greater impact than gamma rays on the noise level. At -15°C, the electronic noise was originally Δ_{noise} = 53 electrons but this will increase to about 71 to 83 electrons when the Astro-H mission ends. This suggests that the BGO energy threshold, currently estimated at $\simeq$100 keV prior to launch [28], may increase by a factor of 1.3$-$1.6, and so the impact of this on background rejection power must be carefully considered prior to launch.

3.4 Verification test

To check the validity of the above theoretical considerations, we measured the energy spectrum of ^{137}Cs using a small BGO scintillator sample (10$\times$10$\times$10 mm^3 in size) coupled with APDs (FM9 and FM10) before and after irradiation. As shown in figure 5 (*top*), the noise only increased slightly for 100-Gy ^{60}Co irradiation, as measured at -15°C, while the FWHM width of the reference test pulse increased slightly from 10.7 to 13.2 keV after irradiation, as measured in BGO-equivalent energy. This 23% degradation in noise performance is almost consistent with expectations for figure 4 (*top*), namely, $\simeq$ 15%. Similarly for the FM9, the FWHM width of the reference test pulse increased from 10.6 to 56.7 keV (by a factor of 5.3), again nearly consistent with our prediction from figure 4 (*bottom*), namely, a factor of 5.1.

There remains a slight mismatch between our expectations and the measurement results, e.g., the measured degradation of noise performance that determines the minimum energy threshold of the BGO readout is always 5 to 10% *worse* than expected than our theoretical considerations. The effect is minor, but may be partially attributable to a slight degradation ($\sim$10%) of the light collection efficiency of APDs after irradiation. Indeed, QE degrades substantially above 600 nm after 100-Gy proton irradiation (figure 3(c)), but it is questionable whether this effect alone can fully explain such a mismatch, since the light emission peak of BGO is $\sim$480 nm and the degraded QE above 600 nm should have little impact. Moreover, QE apparently remained unchanged after 100-Gy gamma ray irradiation (figure 3(c)), although this could be due to certain annealing-related effects. This is because the QE presented in figures 2(c) and 3(c) was measured several months

2012 JINST 7 P06001

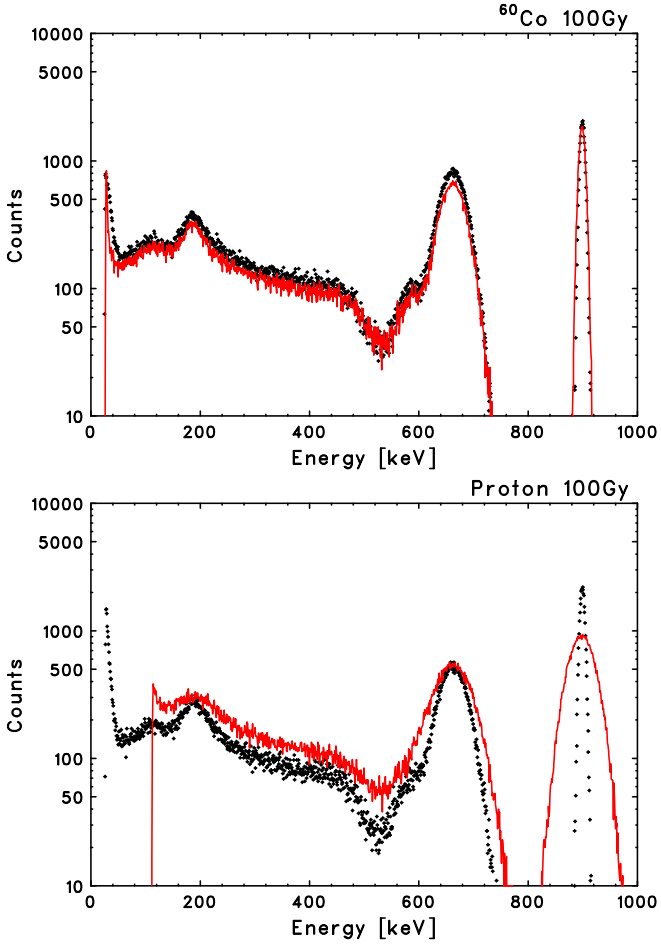

Figure 5. (*top*) (a) Energy spectrum of ^{137}Cs as measured with the FM10 APD coupled to a small BGO scintillator, before (*black*; dots) and after (*red*; line) 100-Gy ^{60}Co irradiation. (*bottom*) (b) Energy spectrum of ^{137}Cs measured with the FM9 APD coupled to a small BGO scintillator, before (*black*; dots) and after (*red*; line) 100-Gy proton irradiation. The measured scintillator sample is $10\times10\times10$ mm^3 in size, and the temperature was fixed at -15°C.

after the irradiation tests, whereas the BGO spectrum was measured much sooner (typically $\sim$24 hours after irradiation).

In this context, we should also mention that the actual dose rate in LEO will be $\simeq (3-6)\times10^{-7}$ Gy/s, clearly much smaller than the dose rate used in the experiments in this paper (0.05 and 0.1 Gy/s for gamma-ray and proton irradiations respectively). The expected radiation damage at such low fluences of protons and electrons is not obvious, since the annealing effect could be important. The dark current may *not* increase linearly with radiation dose, although we assumed a very simple relation in eq. (3.10). Accordingly, we should consider figures 4 (a) and (b) as *conservative*, "worst case" estimates regarding the total dose experienced by APDs in orbit.

Finally, we should also comment on how the performance of the instruments degrades if the cooling system for the HXI or the SGD does not function properly. As we see in eqs. (3.2)

2012 JINST 7 P06001

and (3.3), dark current depends strongly on the operating temperature, with an exponential term $\propto \exp(-\varepsilon/kT)$. Assuming $\varepsilon \simeq 0.6\,\mathrm{eV}$ (see section 3.1), dark current increases by a factor of 1.7 at -10°C, which however results in the degradation of the BGO energy threshold by only 7% (see also figures 2−4). Similarly the BGO energy threshold may increase by a factor of 1.4 for APDs being operated at 0°C, but further deterioration is expected with the radiation damage. Careful temperature control of the APDs in orbit is thus important for both the HXI and SGD instruments aboard Astro-H mission.

4 Conclusion

This paper presented the results of irradiation tests (of both gamma rays and protons) conducted on Hamamatsu reverse-type APDs, which are to be carried aboard the Astro-H mission scheduled for launch in 2014. Based on our theoretical considerations, we successfully distinguished the surface and bulk components of dark current. We also demonstrated that high energy protons cause displacement damage in the bulk material, resulting in a significant increase in bulk current with a change of activation energy, whereas gamma-ray radiation is less damaging as produces an increased surface current. By comparing data obtained at temperatures between -20°C and $+20^{\circ}$C. before and after irradiation, we demonstrated a simple analytical method of estimating the deterioration of electronic noise for APD readout at an arbitrary temperature and radiation dose. As a practical example, we showed that the energy threshold of the BGO readout for Astro-H may increase by a factor of 1.3−1.6 after the expected five-year life of the Astro-H mission. By using a small BGO crystal and irradiating APDs, we showed that our analysis approach can effectively explain the overall trend toward increased noise, to within a 10% accuracy level.

Acknowledgments

We thank the anonymous referee for his/her useful comments and suggestions to improve this manuscript. We wish to thank Drs. Uchibori and Kitamura at HIMAC for their technical support during the collaborative research experiment P258 (proton irradiation to APDs). We also thank Prof. T. Ohsugi, Dr. Y. Fukazawa, and Mr. K. Hayashi for their comments and providing a careful estimate of the radiation dose expected in the Astro-H orbit.

References

[1] P.P. Webb, R.J. McIntyre and J. Conradi, *Properties of avalanche photodiodes*, *RCA Rev.* **35** (1974) 234.

[2] Y. Musienko, *Advances in avalanche photodiodes*, in *Innovative detectors for supercolliders. Proceedings of the* 42nd *Workshop of the INFN ELOISATRON Project*, E. Nappi and J. Seguinot eds., World Scientific, Singapore (2004), pg. 427.

[3] T. Ikagawa et al., *Performance of large-area avalanche photodiode for low-energy X-rays and γ-rays scintillation detection*, *Nucl. Instrum. Meth.* **A 515** (2003) 671.

[4] T. Ikagawa et al., *Study of large area Hamamatsu avalanche photodiode in a γ-ray scintillation detector*, *Nucl. Instrum. Meth.* **A 538** (2005) 640.

2012 JINST 7 P06001

[5] J. Kataoka et al., *Recent progress of avalanche photodiodes in high-resolution X-rays and γ-rays detection*, *Nucl. Instrum. Meth.* **A 541** (2005) 398.

[6] J. Grahl et al., *Radiation hard avalanche photodiodes for CMS ECAL*, *Nucl. Instrum. Meth.* **A 504** (2003) 44.

[7] D. Bailleux et al., *Hamamatsu APD for CMS ECAL: quality insurance*, *Nucl. Instrum. Meth.* **A 518** (2004) 622.

[8] Z. Antunovic et al., *Radiation hard avalanche photodiodes for the CMS detector*, *Nucl. Instrum. Meth.* **A 537** (2005) 379.

[9] Z. Antunovic et al., *Uniformity measurements across the area of the CMS ECAL avalanche photodiodes*, *Nucl. Instrum. Meth.* **A 545** (2005) 139.

[10] M. Bergeron et al., *Performance evaluation of the LabPET^{TM} APD-based digital PET scanner*, *IEEE Nucl. Sci. Symp. Conf. Rec.* **6** (2007) 4185.

[11] D.P. McElroy et al., *Characterization and readout of MADPET-II detector modules: validation of a unique design concept for high resolution small animal PET*, *IEEE Trans. Nucl. Sci.* **52** (2005) 199.

[12] R. Lecomte, *Technology challenges in small animal PET imaging*, *Nucl. Instrum. Meth.* **A 527** (2007) 157.

[13] C. Woody et al., *RatCAP: a small, head-mounted PET tomograph for imaging the brain of an awake RAT*, *Nucl. Instrum. Meth.* **A 527** (2004) 166.

[14] C. Woody et al., *Initial studies using the RatCAP conscious animal PET tomograph*, *Nucl. Instrum. Meth.* **A 571** (2007) 14.

[15] C. Woody et al., *Preliminary studies of a simultaneous PET/MRI scanner based on the RatCAP small animal tomograph*, *Nucl. Instrum. Meth.* **A 571** (2007) 102.

[16] J. Kataoka et al., *Development of large-area, reverse-type APD-arrays for high-resolution medical imaging*, *Nucl. Instrum. Meth.* **A 604** (2009) 323.

[17] J. Kataoka et al., *Development of an APD-based PET module and preliminary resolution performance of an experimental prototype gantry*, *IEEE Trans. Nucl. Sci.* **57** (2010) 2448.

[18] M. Yoshino et al., *The development and performance of UV-enhanced APD-arrays for high resolution PET imaging coupled with pixelized Pr:LuAG crystal*, *Nucl. Instrum. Meth.* **A 643** (2011) 57.

[19] R. Agishev, B. Gross, F. Moshary, A. Gilerson and S. Ahmed, *Simple approach to predict APD/PMT lidar detector performance under sky background using dimensionless parametrization*, *Opt. Lasers Engin.* **44** (2006) 779.

[20] S. Veerabuthiran, A.K. Razdan, M.K. Jindal, D.K. Dubey and R.C. Sharma, *Mie lidar observations of lower tropospheric aerosols and clouds*, *Spectrochim. Acta* **A 84** (2011) 32.

[21] T. Takahashi et al., *The ASTRO-H mission*, *Proc. SPIE* **7732** (2010) 77320Z.

[22] J. Bookbinder, *An overview of the IXO observatory*, *Proc. SPIE* **7732** (2010) 77321B.

[23] J. Kataoka et al., *An active gain-control system for avalanche photo-diodes under moderate temperature variations*, *Nucl. Instrum. Meth.* **A 564** (2006) 300 [astro-ph/0602392].

[24] H. Ashida et al., *Design of Tokyo tech nano-satellite Cute*-1.7 + *APD II and its operation*, in *Proceedings of the* 59th *International Astronautical Congress*, IAC-08-B4.6.A4, http://lss.mes.titech.ac.jp/ssp/cute1.7/paper/iac2008.pdf, Glasgow U.K. September 29– October 3 2008.

2012 JINST 7 P06001

[25] J. Kataoka et al., *In-orbit performance of avalanche photodiode as radiation detector on board the picosatellite Cute-1.7+APD II*, *J. Geophys. Res.* **115** (2010) A05204.

[26] M. Kokubun et al., *Hard X-ray Imager (HXI) for the ASTRO-H mission*, *Proc. SPIE* **7732** (2010) 773215.

[27] H. Tajima et al., *Soft Gamma-ray Detector for the ASTRO-H mission*, *Proc. SPIE* **7732** (2010) 773216.

[28] T. Saito et al., *Development of high performance avalanche photodiodes and dedicated analog systems for HXI/SGD detectors onboard the Astro-H mission*, submitted to *Nucl. Instrum. Meth.* **A** (2012).

[29] H.N. Becker, T.F. Miyahara and A.H. Johnston, *The influence of structural characteristics on the response of silicon avalanche photodiodes to proton irradiation*, *IEEE Trans. Nucl. Sci.* **50** (2003) 1974.

[30] H.N. Becker and A.H. Johnston, *Dark current degradation of near infrared avalanche photodiodes from proton irradiation*, *IEEE Trans. Nucl. Sci.* **51** (2004) 3572.

[31] J. Kodet, I. Prochazka, J. Blazej, X. Sun and J. Cavanaugh, *Single photon avalanche diode radiation tests*, in press *Nucl. Instrum. Meth.* **A** (2012).

[32] J.S. Laird et al., *Effects of gamma and heavy ion damage on the impulse response and pulsed gain of a low breakdown voltage Si avalanche photodiode*, *IEEE Trans. Nucl. Sci.* **53** (2006) 3786.

[33] S. Kasahara, T. Takashima and M. Hirahara, *Variability of the minimum detectable energy of an APD as an electron detector*, *Nucl. Instrum. Meth.* **A 664** (2012) 282.

[34] S.M. Sze, *Physics of semiconductor devices*, 2nd edition, Wiley, New York U.S.A. (1981) [ISBN:047109837X].

[35] T. Ohsugi et al., *Radiation damage in silicon microstrip detectors*, *Nucl. Instrum. Meth.* **A 265** (1988) 105.

[36] J. Kaneko et al., *Improvement of radiation hardness of double-sided silicon strip detector for Belle SVD upgrade*, *IEEE Trans. Nucl. Sci.* **49** (2002) 1593.

[37] Perkin Elmer, *Silicone avalanche photodiodes C30902E, C30902S, C30921E, C30921S, optoelectronics product data sheet*, http://www.htds.fr/doc/optronique/militaireAerospace/SensorsEmittersDetectors.pdf.

[38] M. Moszyn'ski, M. Szawlowski, M. Kapusta and M. Balcerzyk, *Large area avalanche photodiodes in scintillation and X-rays detection*, *Nucl. Instrum. Meth.* **A 485** (2002) 504.

2012 JINST 7 P06001